Article:
Asghar, M.S.A., Inkson, B.J. and Moebus, G. (2017) Giant radiolytic dissolution rates of aqueous ceria observed in-situ by liquid-cell TEM. Chemphyschem, 18 (10). pp. 1247-1251. ISSN 1439-4235

https://doi.org/10.1002/cphc.201601398

A EUROPEAN JOURNAL

CHEMPHYSCHEM

OF CHEMICAL PHYSICS AND PHYSICAL CHEMISTRY

Accepted Article

Title: Giant radiolytic dissolution rates of aqueous ceria observed in-situ by liquid-cell TEM

Authors: Muhammad Sajid Ali Asghar, Beverley J Inkson, and Guenter Moebus

To be cited as: *ChemPhysChem* 10.1002/cphc.201601398

Link to VoR: http://dx.doi.org/10.1002/cphc.201601398

A Journal of

ChemPubSoc Europe

WILEY-VCH

www.chemphyschem.org

Giant radiolytic dissolution rates of aqueous ceria observed in-situ by liquid-cell TEM

Muhammad Sajid Ali Asghar [a], Beverley J. Inkson [a], and Günter Möbus *[a]

Abstract: Dynamics of cerium oxide nanoparticle aqueous corrosion are revealed in-situ. We use innovative liquid-cell transmission electron microscopy (TEM) combined with deliberate high-intensity electron-beam irradiation of nanoparticle suspensions. This enables life video-recording of materials reactions in liquid, with nm-resolution. We introduce image-quantification to measure detailed rates of dissolution as a function of time and particle size to be compared with literature data. Giant dissolution rates, exceeding any previous reports for chemical dissolution rates at room temperature by many orders of magnitude, are discovered. Reasons for accelerated dissolution are outlined, including the importance of radiolysis of water preceding ceria-attack. Electron-water interaction generates radicals, ions and hydrated electrons, which assist in hydration and reductive dissolution of oxide minerals. The presented methodology has the potential to become a novel accelerated testing procedure to compare multiple nanoscale materials for relative aqueous durability. The ceria-water system is of crucial importance for the fields of catalysis, abrasive polishing, environmental remediation, and as simulant for actinide-oxide behaviour in contact with liquid for nuclear engineering.

Irradiation has been frequently used to systematically alter properties of materials, induce changes of physical parameters or patterns and induce chemical reactions [1-3], in addition to emulating radioactive environments [4]. Samples are typically irradiated in a dry state, especially where high vacuum requirements are needed, such as for electron beam irradiation in TEM. Some materials have been identified with exceptional resistance to irradiation damage, amongst them fluorite-structured oxides, e.g. CeO_2, UO_2, ThO_2 and similar [5, 6], which led to the selection of UO_2 as the preferred fission-reactor fuel-rod phase. Detailed irradiation studies of such oxides claim a combination of robustness of the crystal structure with a certain self-healing tendency [7]. In the case of ceria this is based on high oxygen conductivity and tolerance of non-stoichiometry CeO_{2-x} due to the ability of Ce to adjust to oxygen vacancies by reduction to Ce^{3+}. Damage is observed as partial amorphisation, lattice swelling, dislocation formation, and vacancy generation and agglomeration with void formation [8, 9]. Similar to physical robustness, chemical inertness has also been attributed to the CeO_2 family of materials, and while dissolution in hot concentrated hydrochloric acid is well established, research efforts continue very recently to seek for new mixtures of acids, which allow CeO_2 dissolution at lower temperature with milder acid concentrations, which is important for a "green chemistry" agenda, e.g. for recycling and recovery of Ce from within waste car-catalysers [10].

In this context it becomes urgent to study the combination of the two above processes, (i) irradiation of dry ceria, and (ii) wet-chemical dissolution of ceria, into one combined experiment with nanometer scale in-situ observation of wet ceria irradiated in-situ. This has only rather recently been possible thanks to novel "liquid-cell" TEM technology [11, 12]. In such a device, a sub-micron thick water layer is insulated from the TEM-vacuum by being enclosed between two thin amorphous Si-nitride membranes. The electron beam penetrating the sandwich of membranes and water-particle-suspension can be used for the dual purpose of live-imaging at only slightly impaired TEM-resolution, but also for deliberate irradiation studies [13-15]. There are many liquid-cell TEM research efforts dealing with growth of nanoparticles, but only a few of them also mention some observation of dissolution as a secondary effect, including for Au [13, 16] and Ca-carbonate [17]. A Bromine etching study on Pd nanoparticles is presented in [18], while a particle-growth study from Ce-nitrate solution is now also available [19].

Our work aims at introducing liquid cell TEM as a major tool for mainstream dissolution studies, and also providing quantified measurement leading to dissolution rates suitable for comparison. Further, we aim to link the topic through to industrially relevant applications, where knowledge of these dissolution rates is crucial, particularly for cerium oxides.

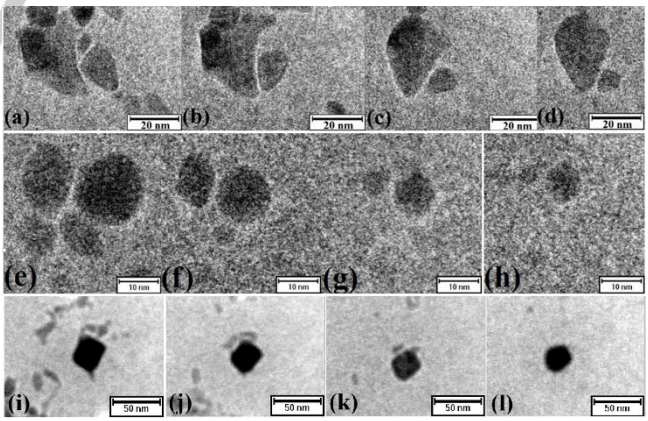

Figure 1. High magnification detail of dynamical dissolution of individual ceria particles, including observations of particle rounding/ corner dissolution (a-d: 6.5 s duration), sphere shrinkage (e-h: 5.2 s duration), and octahedral dissolution (i-l: 28 s duration).

[a] Mr. M.S. Ali Asghar , Prof. B. J. Inkson and Dr. G. Möbus
Department of Materials Science and Engineering
University of Sheffield
Mappin Street, Sheffield, S1 3JD, UK
E-mail: m.sajid@sheffield.ac.uk , beverley.inkson@sheffield.ac.uk
and g.moebus@sheffield.ac.uk

Previous studies in the area of CeO_2/H_2O interactions or their actinide equivalent were mostly motivated by: (i) behaviour of nuclear fuel rods in contact with neutron-moderation or cooling water, during operation or accidents [20, 21], (ii) behaviour of directly disposed nuclear waste of UO_2 phase without vitrification, for which the very long term surface reaction with water over

thousands of years and slow dissolution is targeted [22, 23], (iii) CeO_2 waste nanoparticles, e.g. released to the environment due to their incorporation in household products or as car fuel additives, and their long-term stability in earth/water systems [24], (iv) the aggressive recovery of Ce during ceria recycling [25]. Within those four separate research fields all involving ceria-dissolution, it should be noted, that (i) and (ii) share high levels of irradiation, while (iii) and (iv) do not. On the other hand, (i) and (ii) operate on macroscopic, e.g. sintered materials quantities, while (iii) and (iv) involve nanoparticles or nanostructured (e.g. porous) ceria materials. There is further interest in the ceria/water system in research areas of catalysis, without attempted dissolution [26].

Further potential applications include (v) environmental clean-up of organic waste in water through photocatalysis with or without irradiation [27], and (vi) engineered water-splitting as part of hydrogen-production or syngas conversion in large-scale catalytic reactor research [28].

Here we focus on the irradiation behaviour of Ce-oxide nanoparticles dispersed in distilled water (Fig 1). The ceria [Sigma-Aldrich UK] is predominantly of size-range of 10-40 nm diameter and apart from roundish and irregular shaped particles it contains a significant portion of octahedral shape, as described previously [29]. Stability of the nanoparticles is found to show remarkable irradiation-intensity dependence which can be user-adjusted by varying the electron beam diameter (see also experimental section).

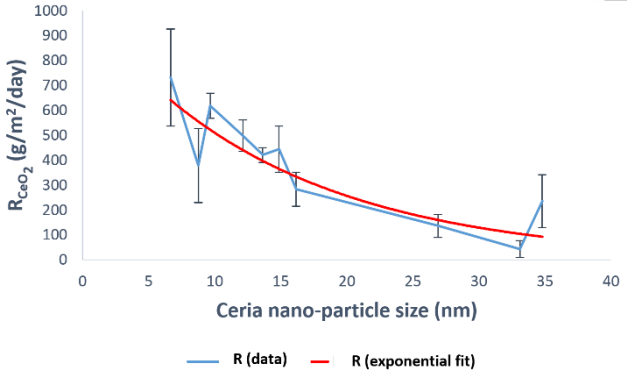

Figure 2. Measured ceria dissolution rates as function of instantaneous particle size along with exponential model.

(i) At low-level intensity, as typically used for imaging, extended time-series observation of ceria nanoparticles is possible, which allows e.g. the study of particle movements, particle aggregation and attachment, as well as tracking of individual particles in 3D. Particle movement is triggered by irradiation or via short syringe-supply of fresh water to shake up any settled particles. Such results will be reported in a future paper.

(ii) Dissolution of corners or edges leading to a significant rounding of originally irregular or facetted crystalline particles (Fig 1a-d).

(iii) Shrinkage of the particle diameter, which can be tracked continuously and, for regular shaped particles quantified by calibrating to volume loss per momentary surface area (Fig 1e-h, and i-l).

By reducing electron beam intensity, the dissolution process can be slowed-down/halted at any time, while still providing enough intensity for imaging. As it has been reported that CeO_2 dissolution rate depends on nanoparticle size [24], we quantify the dissolution rate as function of particle radius. The graph of Fig 2 is a composite of tracking two particles, the error bars account for 5 repeat measurements in multiple aspects for each time-step. Our dissolution rates R are calculated from time differences in volume and normalised to the initial surface area at the start of the interval, where m_D indicates dissolved mass, ρ density of CeO_2, V_{SNP} and A_{SNP} the volume and surface area in spherical nanoparticle approximation, at time interval t_n. Units of g/m^2/day are used for R due for comparison with earlier literature.

$$m_D = \rho\,(V_{SNP}(t_n) - V_{SNP}(t_{n-1})) \quad (1)$$

$$R\,(t_n) = m_D / A_{SNP}(t_{n-1}) / (t_n - t_{n-1}) \quad (2)$$

Due to the change in particle radius during dissolution, the dissolution rate R becomes a function of both radius and time, unlike for flat surfaces. The fit seems to well approximate an exponential increase with radius and decrease with time, where α,β,γ are fitting constants and r_0 is the initial particle radius:

$$R\,(r,t) = \alpha\, exp\,(-\beta\, r(t)) \quad (3)$$

$$r = r_0 - \gamma t \quad (4)$$

$$R\,(t) = \alpha\, exp\,(-\beta\,(r_0 - \gamma t)) = const \cdot exp\,(\beta\gamma t) \quad (5)$$

In this case the particle radius shrinks from 35 nm to 5nm, which corresponds to an exponent β = 0.069 in eq. 3, while the speed of shrinkage by radius amounts to γ = 0.91 nm/s, surprisingly well linear. Beyond the continuous tracking of particles NP1 and NP2 in Figs 1-2, some further particles have been quantified, and the results of all 5 particles included in table 1. This table also includes literature ex-situ chemical measurements, in order to put our measured dissolution rates into context. Dissolution rates are found to vary from ~ 10 – 700 g/m^2/day, but generally they are at least 5 orders of magnitude greater than those reported earlier. Particle shape seems to be of minor influence.

Table 1. Comparison of ceria dissolution rates from literature with samples from this work (NP1-5).

Ref	Temp (°C)	Dissolution $R(CeO_2)$ (g/m^2/d)	Comments
[10]	40	1.8 x10-8	Ceria NPs, 0.25 M HNO_3 & Pt NPs (2.5 wt%)
[25]	40	2.7 x10-9	Ceria NPs, 0.125 M H_2SO_4 with ultrasound (20kHz) & Pt NPs
[30]	60	2.9 x10-5	Macro-ceria, 2 M HNO_3
[22]	90	4.85 x10-4	Macro-ceria, 0.01 M HNO3
NP 1	RT	43 - 235	Min – Max rate (Round shape)
NP 2	RT	283 - 730	Min – Max rate (Round shape)
NP 3	RT	28 - 157	Min – max (Octahedral shape)
NP 4	RT	18 - 122	Min – max (Oval shape)
NP 5	RT	7 - 130	Min – max (Octahedral shape)

Irradiation physics of water under electron beams is discussed for the case of distilled water in [16, 31] and for solutions with dissolved precursor chemicals in [32, 33]. Water splitting generates ionic species of both alkaline and acidic character. Following the modelling of the time development in [16], as we use pure deionised water, ultimately H_3O^+ generation dominates,

causing a drop in pH down to around 3. We therefore assume acidic dissolution.

The dissolution process can be understood as a reversed precipitation and derived from well-published pH-base phase diagrams. Karakoti et al. [34] and Ikeda-Ohno et al. [35] have experimentally explored Ce^{IV} speciation over the full pH range from 0 to 14, finding two important thresholds: Above pH=3 precipitation of CeO_2 occurs, while between pH=0.5-3, Ce^{IV} is complexed in solution surrounded by (OH^-) groups, and below pH=0.5 Ce^{IV} is directly solvated. It is therefore likely that by reversion the Ce^{IV} ions are liberated through hydrolysis and kept in solution as hydroxylated ions. Whether the ions maintain their valence as Ce^{IV} in the raw particles and in solution, depends on the electron beam interaction with water and on the chemical stability as revealed in its Pourbaix diagram [36]. Such diagram predicts stability of Ce^{III} vs Ce^{IV} as well as stability of Ce^n vs $Ce(OH)_n$ as function of electrochemical potential E and pH value. For de-ionised water as our starting point, H_3O^+ generation during irradiation [16] would move the system quickly into low pH and therefore a high ionic solution range. Simultaneously, the incident electron beam generates further electrons (low-energy secondary electrons in any solid/liquid and more specifically bound hydrated electrons in water) plus further H_2O-derived radical species and gases (H_2, O_2) [31] throughout the interaction volume. Eventually, the system will respond with secondary phase precipitation events (to be reported in future work).

Discussion of the origin of the giant dissolution rates, which appear 5 orders of magnitude higher than any reported room temperature rates for ceria of any morphology, has to consider 6 key effects one-by-one: (i) molarity/acidity, (ii) temperature, (iii) particle size, (iv) particle microstructure, (v) reactive water splitting products, and (vi) catalytic oxide action.

(i) a scaling phenomenon with respect to acidic molarity is unlikely: Extrapolating literature data for 1M and 2M HNO_3 dissolution of CeO_2 [10], as well as from 0.5M to 6M [30], indicates that rate changes are confined to a factor 10 within 12 times higher molarity. Even if a linear relationship does not hold, 5 orders of magnitude higher R-rates cannot be reached via such a pure H_3O^+ increase alone.

(ii) a water temperature influence with a factor 2 in ceria dissolution rate for 30º temperature rise was reported [30]. Comparing thermal conductivity of water with solids reported before, water-temperature rise can be safely limited to below 5 degrees [37, 38], therefore we can safely discard this option.

(iii) nanoparticle size has been confirmed via Fig 2 to play a role within 1 order of magnitude, compatible with [10], but cannot bridge five orders. In fact the dissolution rate measurements summarized in Table 1 include a range of material sizes, from nanoparticles of few tens of nm [10] to high-temperature sintered solid bulk materials as for simulated nuclear waste scenarios [22, 30]. Differences are again within 2 orders of magnitude, not enough to explain the giant rates.

(iv) materials microstructure and defects have been highlighted to have prominent influence in [30], but again not beyond one order of magnitude. Indeed, our live observations confirm primary dissolution of octahedral edges with high surface energy, before dissolution of the rounded remaining core of particles proceeds. As the surface energy is inverse to radius of curvature, accelerated dissolution as of Fig 2 is expected.

(v) this leaves reactive water splitting products as the likely explanation, as these reactants/radicals are not or less present in any of the literature experimental set-ups. Here irradiation is via a high density of electrons with moderate electron energy (300kV). In comparison radioactive decay in the case of UO_2/ThO_2 dissolution studies would contribute much lower background irradiation dose, but with higher particle energies. The additional reactive species in radiolytic water, which would be absent in standard acidic solutions, include, amongst others [16, 31], hydrated electrons (first milliseconds only [16]), hydrogen (the main reducing agent), oxygen, H_2O_2, as well as radicals of hydrogen, water, and hydroxide.

(vi) considering alternative scenarios, we mention the possibility in which irradiation "activates" CeO_2 by generating CeO_{2-x} and Ce^{3+}, especially on nanoparticle surfaces. Subsequently CeO_{2-x} could split water catalytically [39], as proposed for commercial ceria-based H_2-production set-ups. Similarly for ceria or zirconia coatings, H_2-production via oxide-assisted water splitting has also been established under gamma-irradiation in a nuclear fission context [40]. However, both scenarios consider thin H_2O layers adsorbed on an oxide majority-phase, and do not assume H_2-production to trigger oxide-dissolution. Other evidence against this effect being of importance, is the dose-dependence we observe. This can only be explained by direct water-splitting through e-beam-water interaction, independent of the available ceria-surface area (which would decline while our dissolution rates go up).

In summary, we discovered an effect of radiolytic dissolution of ceramic oxides, which exhibits dissolution rates as never reported before. This could evolve into a useful technology of "accelerated testing" of oxide durability in aqueous environment via quantitatively measuring and live-tracking of dissolution rates, and could be very valuable for various research and application fields: (i) Ultra-rapid screening of materials-series, e.g. various ceria-doping levels, comparison of multiple fluorite-oxides, or multiple lanthanide oxides for longevity in liquids or under irradiation, (ii) prediction of long-term stability and durability of particles in chemically acidic environments, (iii) usage of oxide coatings for nuclear engineering of fission fuel assemblies; (iv) new options for rapid room-temperature dissolution of ceria within a cerium-recycling agenda are opened-up avoiding strong acids and high temperatures. More generally, no other technique is known which provides such high spatial resolution in modifying chemical activity laterally on a scale of sub-micron liquid volume. Changing of beam diameter will vary dissolution rates as desired. True nano-chemistry becomes possible as pH value and reactivity of a liquid host can be changed within sub-second duration. And this excellent localisation is combined with the in situ imaging and measurement capability of sub-TV-rate video observation and imaging resolution of ~ sub-nm, enabling fascinating insight into the kinetics of dissolution which have never been observed with such high detail before.

Experimental Section

Irradiation is carried out using a 300kV LaB_6 TEM (model JEOL JEM 3010). The particles are directly loaded by a small droplet to the electron transparent area of the sample-sandwich, which consists of two Si_3N_4 membranes. In addition a fresh distilled water supply to the sample area during TEM sessions, is provided via syringe load to the tubing of the specimen holder (model Protochips-Poseidon [41]). Once the current density exceeds a transition value, the ceria particles are subjected to continuous dissolution. A typical measured density value was around ~ 3 nA/μm^2 on the sample, corresponding to 35 nA beam current with a beam diameter of 4 μm. The transition intensity value will depend on the thickness of the water layer, which can locally vary due to bending of the Si_3N_4 membranes.

Acknowledgements

We thank NED University of Engineering and Technology, Pakistan, The University of Sheffield, UK, and EPSRC, UK (EP/J021199/1) for funding parts of this project.

Keywords: Liquid-Cell TEM • Corrosion • Radiolysis • Cerium oxide • Durability

[1] M. E. Mochel, C. J. Humphreys, J. A. Eades, J. M. Mochel and A. M. Petford, *Appl. Phys. Lett.* **1983**, 42, 392-394.
[2] J. Lian, L. M. Wang, K. Sun and R. C. Ewing, *Micr. Res. Techn.* **2009**, 72, 165-181.
[3] J. A. Hinks and P. D. Edmondson, *J. Appl. Phys.* **2012**, 111, 053510 (1-7).
[4] F. Granberg, K. Nordlund, M. W. Ullah, K. Jin, C. Lu, H. Bei, L. M. Wang, F. Djurabekova, W. J. Weber and Y. Zhang, *Phys. Rev. Lett.* **2016**, 116, 135504 (1-8).
[5] A. Debelle, S. Moll, B. Decamps, A. Declemy, L. Thome, G. Sattonnay, F. Garrido, I. Jozwik and J. Jagielski, *Scripta Materialia* **2010**, 63, 665-668.
[6] K. Yasunaga, K. Yasuda, S. Matsumura and T. Sonoda, *Nucl Instr Method Phys Res B.* **2006**, 250, 114-118.
[7] Y. Zhang, P. D. Edmondson, T. Varga, S. Moll, F. Namavar, C. Lan and W. J. Weber, *Phys. Chem. Chem. Phys.* **2011**, 13, 11946-11950.
[8] U. M. Bhatta, F. Karounis, A. Stringfellow and G. Möbus, *MRS Proceedings* **2013**, 1552, 125-130..
[9] T. S. Sakthivel, D. L. Reid, U. M. Bhatta, G. Möbus, D. C. Sayle and S. Seal, *Nanoscale* **2015**, 7, 5169-5177.
[10] M. Virot, T. Chave, D. Horlait, N. Clavier, N. Dacheux, J. Ravaux and S. I. Nikitenk, *J. Mater. Chem.* **2012**, 22, 14734–14740.
[11] M. J. Williamson, R. M. Tromp, P. M. Vereecken, R. Hull and F. M. Ross, *Nature Materials* **2003**, 2, 532-6.
[12] N. De Jonge and F. M. Ross, *Nature Nanotechnology* **2011**, 6, 695-704.
[13] J. Hermannsdorfer, N. D. Jonge and A. Verch, *Chem. Commun.* **2015**, 51, 16393-16396.
[14] H. G. Liao, K. Niu and H. Zheng, *Chem Commun* **2013**, 49, 11720-7.
[15] H.-G. Liao, L. Cui, S. Whitelam and H. Zheng, *Science* **2012**. 336, 1011-1014.
[16] N. M. Schneider, M. M. Norton, B. J. Mendel, J. M. Grogan, F. M. Ross and H. H. Bau, *J. Phys. Chem. C* **2014**, 118, 22373-22382.
[17] M. H. Nielsen, S. Aloni and J. J. De Yoreo, *Science* **2014**, 345, 1158-1162.
[18] Y. Jiang, G. Zhu, F. Lin, H. Zhang, C. Jin, J. Yuan, D. Yang and Z. Zhang, *Nano Lett* **2014**, 14, 3761-5.
[19] P. Abellan, T. H. Moser, I. T. Lucas, J. W. Grate, J. E. Evans and N. D. Browning, *RSC Adv.* **2017**, 7, 3831-3837.
[20] F. N. Skomurski, L. C. Shuller, R. C. Ewing and U. Becker, *Journal of Nuclear Materials* **2008**, 375, 290–310.
[21] S. Sunder and N. H. Miller, *Journal of Nuclear Materials* **2000**, 279, 118-126.
[22] M. C. Stennett, C. L. Corkhill, L. A. Marshall and N. C. Hyatt, *Journal of Nuclear Materials* **2013**, 432, 182–188
[23] C. L. Corkhill, D. J. Bailey, F. Y. Tocino, M. C. Stennett, J. A. Miller, J. L. Provis, K. P. Travis and N. C. Hyatt, *Appl. Mater. Interfaces* **2016**, 8, 10562−10571.
[24] J. T. Dahle, K. Livi and Y. Arai, *Chemosphere* **2015**, 119, 1365-1371.
[25] X. Beaudoux, M. Virot, T. Chave, G. Leturcq, N. Clavier, N. Dacheux and S. I. Nikitenko, *Hydrometallurgy* **2015**, 151, 107–115.
[26] M. Molinari, S. C. Parker, D. C. Sayle and M. S. Islam, *J. Phys. Chem. C* **2012**, 116, 7073−7082.
[27] M. M. Khin, A. S. Nair, V. J. Babu, R. Murugana and S. Ramakrishna, *Energy Environ. Sci.* **2012**, 5, 8075-8109.
[28] F. Lemont, *International Journal of hydrogen energy* **2008**, 33, 7355-7360.
[29] X. Xu, Z. Saghi, R. Gay and G. Möbus, *Nanotechnology* **2007**, 18, 225501 (1-8).
[30] L. Claparede, N. Clavier, N. Dacheux, P. Moisy, R. Podor and J. Ravaux, *Inorg. Chem.* **2011**, 50, 9059–9072.
[31] S. L. Caër, *Water* **2011**, 3, 235-253.
[32] J. H. Park, N. M. Schneider, J. M. Grogan, M. C. Reuter, H. H. Bau, S. Kodambaka and F. M. Ross, *Nano Lett* **2015**, 15, 5314-20.
[33] P. Abellan, B. L. Mehdi, L. R. Parent, M. Gu, C. Park, W. Xu, Y. Zhang, I. Arslan, J. G. Zhang, C. M. Wang, J. E. Evans and N. D. Browning, *Nano Lett* **2014**, 14, 1293-9.
[34] A. S. Karakoti, S. V. N. T. Kuchibhatla, K. S. Babu and S. Seal, *J. Phys. Chem. C* **2007**, 111, 17232-17240.
[35] A. Ikeda-Ohno, C. Hennig, S. Weiss, T. Yaita and G. Bernhard, *Chem. Eur. J.* **2013**, 19, 7348 – 7360.
[36] P. Yu, S. A. Hayes, T. J. O'Keefe, M. J. O'Keefe and J. O. Stoffer, *Journal of The Electrochemical Society* **2006**, 153, C74-C79.
[37] G. Möbus, M. Ojovan, S. Cook, J. Tsai and Y. Guang, *Journal of Nuclear Materials* **2010**, 396, 264-271.
[38] S. B. Fisher, *Radiation Effects* **1970**, 5, 239–243.
[39] H. A. Hansen and C. Wolverton, *J. Phys. Chem. C* **2014**, 118, 27402−27414.
[40] J. A. Laverne and L. Tandon, *J. Phys. Chem. B* **2002**, 106, 380-386.
[41] K. L. Klein, I. M. Anderson and N. De Jonge, *J. Microsc.* **2011**, 242, 117–123.

Entry for the Table of Contents (Please choose one layout)

Layout 1:

COMMUNICATION

Text for Table of Contents

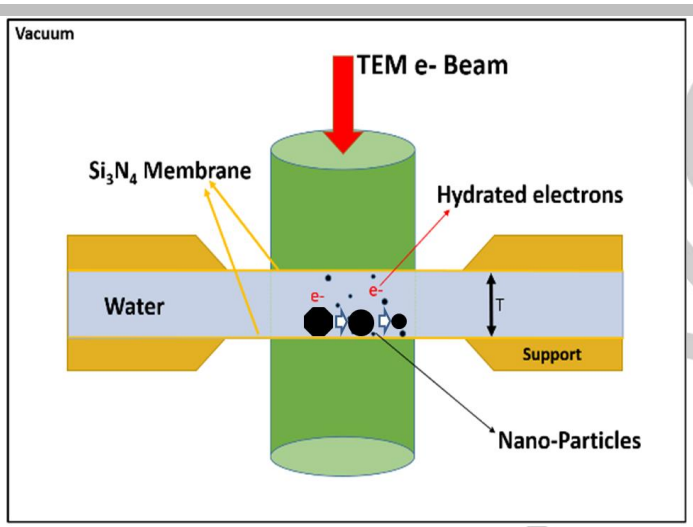

*Author(s), Corresponding Author(s)**

Page No. – Page No.

Title

Layout 2:

COMMUNICATION

((Insert TOC Graphic here))

*Author(s), Corresponding Author(s)**

Page No. – Page No.

Title

Text for Table of Contents